Li *et al. Chem. Synth.* **2025**, *5*, 29
DOI: 10.20517/cs.2024.127

Chemical Synthesis

Research Article

Open Access

Check for updates

Up-conversion effect boosted NIR-driven photocatalytic solar fuel generation of $NaYF_4$: Yb, Er decorated $ZnIn_2S_4$ flowers with rich Zn vacancies

Xuejing Li[1,#], Haiyue Wu[1,#], Shengyan Yin[2], Chenhao Yu[2], Yongzhi Shao[2], Donglei Zhou[2,*], Ping She[1,2,*]

[1]State Key Laboratory of Inorganic Synthesis and Preparative Chemistry, College of Chemistry, International Center of Future Science, Jilin University, Changchun 130012, Jilin, China.
[2]State Key Laboratory of Integrated Optoelectronics, College of Electronic Science and Engineering, Jilin University, Changchun 130012, Jilin, China.
[#]Authors contributed equally.

[*]**Correspondence to:** Dr. Ping She, State Key Laboratory of Inorganic Synthesis and Preparative Chemistry, College of Chemistry, International Center of Future Science, Jilin University, 2699 Qianjin Street, Changchun 130012, Jilin, China. E-mail: sheping@jlu.edu.cn; Dr. Donglei Zhou, State Key Laboratory of Integrated Optoelectronics, College of Electronic Science and Engineering, Jilin University, Jilin University, 2699 Qianjin Street, Changchun 130012, Jilin, China. E-mail: zhoudl@jlu.edu.cn

How to cite this article: Li, X.; Wu, H.; Yin, S.; Yu, C.; Shao, Y.; Zhou, D.; She, P. Up-conversion effect boosted NIR-driven photocatalytic solar fuel generation of $NaYF_4$: Yb, Er decorated $ZnIn_2S_4$ flowers with rich Zn vacancies. *Chem. Synth.* **2025**, *5*, 29. https://dx.doi.org/10.20517/cs.2024.127

Received: 8 Sep 2024 **First Decision:** 30 Sep 2024 **Revised:** 16 Oct 2024 **Accepted:** 23 Oct 2024 **Published:** 25 Feb 2025

Academic Editor: Jin Xie **Copy Editor:** Pei-Yun Wang **Production Editor:** Pei-Yun Wang

Abstract

Photocatalytic CO_2 reduction for solar fuel generation is a promising approach to alleviating the environmental and energy crisis. Herein, a flower-like composite was obtained by assembling Zn vacancy-rich $ZnIn_2S_4$ (V_{Zn}-ZIS) with up-conversion nanoparticles (UCNPs, $NaYF_4$: Yb, Er). Specifically, the optimized UCNPs@V_{Zn}-ZIS demonstrates superior CO generation of 32.57 μmol/g in the near-infrared (NIR)-driven photocatalytic CO_2 reduction process within 8 h. Fortunately, the performance of photocatalytic CO_2 reduction based on optimized UCNPs@V_{Zn}-ZIS is superior to most reported photocatalysts under NIR irradiation. The enhanced photocatalytic CO_2 reduction activity is attributed to the extended light absorption, enhanced charge separation, and improved CO_2 activation of the surface vacancy. The work presented here provides a facile approach to developing novel broad spectral responsive photocatalytic CO_2 reduction photocatalysts, which hold great potential for solar fuel generation in future applications.

Keywords: Photocatalysis, $ZnIn_2S_4$ (ZIS), up-conversion, vacancies, CO_2 reduction

INTRODUCTION

Nowadays, the energy crisis and environmental pollution issues are becoming increasingly serious with the rapid development of industrial society[1,2]. Great efforts have been devoted to the long-term development of human society. The photocatalytic reduction of CO_2 into high-value-added chemicals is a promising approach to alleviating the environmental and energy crisis[3,4]. However, photocatalytic CO_2 reduction efficiency suffers from unsatisfied light harvesting, fast combination of charge carriers, low reaction activity, and poor selectivity[5-7]. Therefore, the rational design of efficient photocatalytic CO_2 reduction photocatalysts is of great significance in photocatalysis. It has been reported that visible and near-infrared (NIR) light account for about 45% and 50% of the total solar spectrum, respectively[8]. Compared with visible light, NIR light possesses a larger proportion, enhanced penetration depth, reduced absorption competition, and fewer side reactions, which will activate photocatalysts uniformly and increase the absorption and utilization of solar energy[9]. Among various photocatalytic CO_2 reduction catalysts, $ZnIn_2S_4$ (ZIS) is a typical transition metal sulfide, which has drawn increasing attention based on great visible light harvesting, tunable morphology, and environmental friendliness properties[10-13]. However, the potential of utilizing ZIS as a NIR-responsive photocatalyst is rarely reported.

Tremendous strategies have been devoted to developing NIR-responsive photocatalysts. Among these approaches, modifying lanthanide-doped up-conversion nanoparticles (UCNPs) on the surface of semiconductors is considered an efficient approach to broaden the light-harvesting region[14-16]. In detail, the doping of rare earth ions can reduce the band gap of semiconductors, which can extend the light absorption into the NIR region. Specifically, the UCNP materials (e.g., $NaYF_4$: Yb, Er) can absorb the low-energy photons (NIR) and emit high-energy photons (Ultraviolet or visible light) through the process of anti-stokes shift luminescence[17]. As a result, the emission of the UCNP materials can facilitate the generation of photo-induced electron-hole pairs for further photocatalytic applications. In detail, Yu *et al.* coupled UCNPs ($NaYF_4$: Yb, Tm) with hierarchical ZIS nanorods as a NIR-responsive photocatalyst for photocatalytic CO_2 reduction, which demonstrates the CO generation rate of 1,500 nmol/g/h[18]. It has been reported that UCNP materials have been utilized to combine with various semiconductors [such as TiO_2, ZnO, and metal-organic frameworks (MOFs)], which often exhibit superior NIR-driven photocatalysis or photodynamic therapy[19-22]. However, it is still difficult to realize highly efficient photocatalytic CO_2 reduction of the composites of UCNPs@semiconductor. Hence, it is of great meaning to develop highly efficient NIR-driven photocatalytic CO_2 reduction photocatalysts based on up-conversion approaches.

Recently, introducing vacancies into the surface of photocatalysts has drawn increasing attention[23-25]. The introduced vacancy can generate a new energy level, which can improve photocatalytic activity due to extended light absorption and facilitated charge carrier separation[26]. Additionally, it can work as a reaction site, which can ameliorate the charge density distribution and reduce the reaction energy barrier of CO_2 reduction[27]. Furthermore, the morphology control plays an important role in photocatalytic performance. Specifically, a hierarchical nanosheet assembled structure is favorable for the reduced diffusion distance for charge transportation when compared with bulk ones[28]. Therefore, it is a promising approach to develop nanosheet-assembled nanocatalysts with surface vacancy sites for much more efficient photocatalysis.

Herein, a NIR-responsive flower-like UCNPs@Zn vacancy-rich ZIS (V_{Zn}-ZIS) photocatalyst was developed by assembling UCNPs on nanosheet-assembled ZIS with rich zinc vacancies, which demonstrated superior CO evolution of 32.57 μmol/g under NIR light irradiation for 8 h. Moreover, the detailed photocatalytic CO_2 reduction mechanism over UCNPs@V_{Zn}-ZIS is investigated by detailed characterization techniques. The elevated photocatalytic CO_2 reduction performance is contributed by enhanced light harvesting and facilitated photo-induced charge separation. The facile design presented here holds great potential for NIR-driven solar fuel generation.

EXPERIMENTAL

Chemicals

Glycerol (Tianjin Fuyu Chemical Co., Ltd., AR); Deionized water (DI water); Ethanol (Tianjin Jingdongtianzheng Precision Chemical Reagent Factory, AR); Anhydrous Zinc chloride ($ZnCl_2$, Innochem, 98%); Indium chloride trihydrate ($InCl_3 \cdot 4H_2O$, Innochem, 99.99%); Thioacetamide (TAA, Innochem, ≥ 98%); Sodium hydroxide (NaOH, Tianjin Guangfu Fine Chemical Co., Ltd.); Ammonium Fluoride (NH_4F, Fuchen Chemical Reagent Co., Ltd.); Methyl Alcohol (Anhui Tedia High Purity Solvents Co., Ltd., AR); Erbium chloride hexahydrate ($ErCl_3 \cdot 6H_2O$, Innochem, 99.99%); Ytterbium chloride hexahydrate ($YbCl_3 \cdot 6H_2O$, Innochem, 99.99%); Yttrium chloride hexahydrate ($YCl_3 \cdot 6H_2O$, Innochem, 99.9%); Octadecene (Innochem, 90%); Oleic Acid (Aladdin, AR); Cyclohexane (Innochem, 99.7%).

Preparation of ZIS

The detailed synthesis procedures were described in Supplementary Materials.

Preparation of V_{Zn}-ZIS

V_{Zn}-ZIS was synthesized according to the previous literature[26]. The detailed procedures were described in Supplementary Materials.

Preparation of UCNPs

The detailed synthesis procedures were described in Supplementary Materials.

Preparation of UCNPs@V_{Zn}-ZIS

The UCNPs@V_{Zn}-ZIS composite was synthesized using a facile physical mixing method. Specifically, masses of V_{Zn}-ZIS and UCNPs were weighted separately and ground in a mortar for 5 min.

Characterizations

The characterization details were provided in the Supplementary Materials.

Electrochemical and photoelectrochemical characterizations

Electrochemical impedance spectroscopy (EIS), Photocurrent response, and Mott-Schottky (MS) measurements were conducted on a CHI660E electrochemical workstation with a standard three-electrode cell. Specifically, the Pt wire and Ag/AgCl electrode were selected as the counter electrode and reference electrode, respectively. As for the working electrode, 5 mg of V_{Zn}-ZIS was added to the mixture of ethanol (200 μL) and Nafion (20 μL). After sonicating the solution for several minutes, the catalyst was dropped on an indium tin oxide (ITO) glass with a controlled area of 1 cm^2. The working electrode was obtained and then dried in air for 2 h. Photocurrent response was obtained using a 300 W Xe lamp as the light source.

Photocatalytic experiments

Photocatalytic CO_2 reduction experiments were conducted in a 35 mL photocatalytic bottle under a Xe lamp with a cut-off filter ($\lambda > 800$ nm). Generally, 5 mg of photocatalyst was added into 10 mL of 0.1 M TEOA anhydrous acetonitrile. Before photocatalysis, high-purity CO_2 gas was purged into the bottle for 20 min to remove the air. The photocatalytic CO_2 reduction reaction was conducted under NIR light (PCX50C; China Education Au-light) with continuous stirring. At each time interval, 200 μL of gas was extracted and injected into a gas chromatograph (GC-2014) to analyze the composition and content of the gaseous product.

Figure 1. The synthesis procedure of composite of UCNPs@V_{Zn}-ZIS. UCNPs: Up-conversion nanoparticles; V_{Zn}-ZIS: Zn vacancy-rich $ZnIn_2S_4$.

RESULTS AND DISCUSSION

Photocatalyst preparation

The synthesis procedure of UCNPs@V_{Zn}-ZIS is shown in Figure 1. Specifically, V_{Zn}-ZIS was prepared by a hydrothermal approach. The UCNPs ($NaYF_4$: 20% Yb, 2% Er) were synthesized using a hydrothermal method under an Ar atmosphere. Subsequently, the composite of UCNPs@V_{Zn}-ZIS was obtained via a physical mixing approach.

Morphologies and characterizations

The morphology of samples was investigated using scanning electron microscopy (SEM), transmission electron microscopy (TEM), and high-resolution TEM (HRTEM) measurements. As shown in Figure 2A, V_{Zn}-ZIS demonstrates a nanosheet-assembled nanoflower-like morphology. As shown in the HRTEM image of V_{Zn}-ZIS in Figure 2B, the lattice fringe of 0.32 nm can be assigned to the (102) plane of ZIS. In addition, the discontinuous and distorted lattice fringes (in yellow circles) demonstrate the existence of vacancies in V_{Zn}-ZIS[29]. The prepared UCNPs were well-arranged nanoparticles, which can also regularly stack into pieces [Figure 2C]. In addition, the TEM image of UCNPs demonstrates a hexagonal shape with a size of about 20 nm [Supplementary Figure 3C]. As a result, the composite of UCNPs@V_{Zn}-ZIS exhibits the same flower-like morphology as V_{Zn}-ZIS with UCNPs decorated in petals [Figure 2D]. Furthermore, the yellow circle in the TEM image of UCNPs@V_{Zn}-ZIS [Figure 2E] also proves the existence of UCNPs on V_{Zn}-ZIS. In Figure 2F, the lattice fringe spacing of 0.29, 0.32, and 0.41 nm can be assigned to (104), (102), and (006) planes of hexagonal ZIS, accordingly[30,31]. The lattice fringe spacing of 0.51 nm belonged to the (100) plane of UCNPs[32]. Therefore, the coexistence of ZIS and UCNPs proves the successful preparation of UCNPs@V_{Zn}-ZIS. Additionally, The SEM element mapping images [Figure 2G] prove the uniform dispersion of Na, Y, F, Yb, Er, Zn, In, and S elements in UCNPs@V_{Zn}-ZIS.

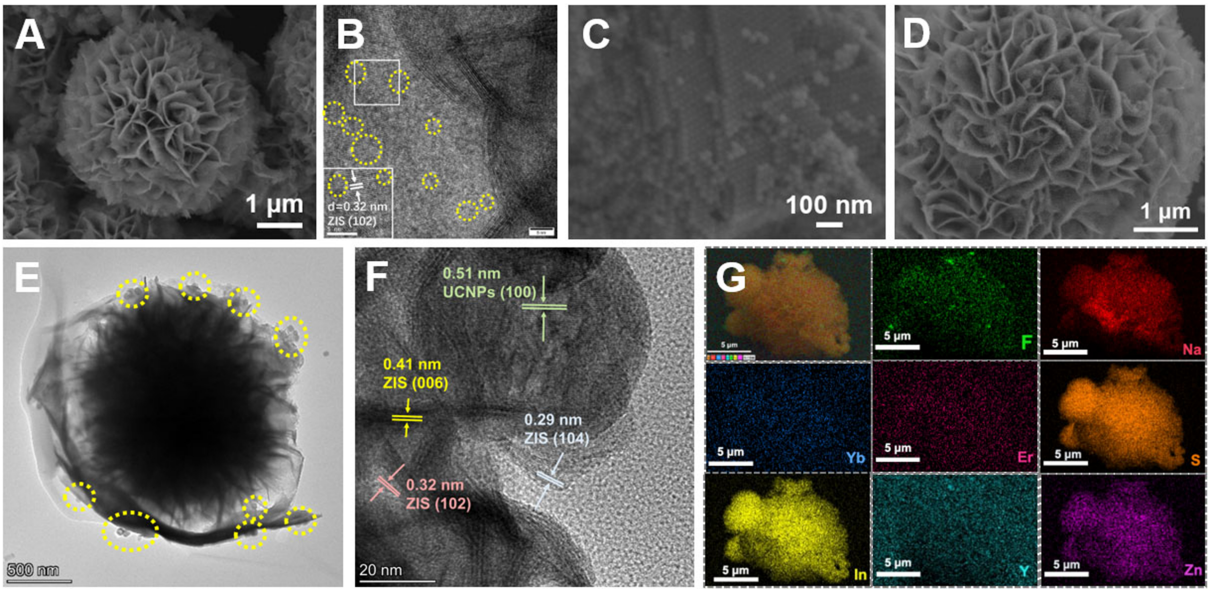

Figure 2. (A) SEM image and (B) HRTEM image of V_{Zn}-ZIS; (C) SEM image of UCNPs; (D) SEM, (E) TEM image, (F) HRTEM image and (G) SEM element mapping images of UCNPs@V_{Zn}-ZIS. SEM: Scanning electron microscopy; HRTEM: high-resolution transmission electron microscopy; V_{Zn}-ZIS: Zn vacancy-rich $ZnIn_2S_4$; UCNPs: up-conversion nanoparticles; TEM: transmission electron microscopy.

As shown in Figure 3A, X-ray diffraction (XRD) patterns of V_{Zn}-ZIS and ZIS are consistent with the reported hexagonal ZIS[33]. In addition, the diffraction peaks of UCNPs follow the relevant standard PDF card (No. 16-0334), proving the successful preparation of UCNPs. Moreover, the XRD patterns of UCNPs@V_{Zn}-ZIS exhibit characteristic peaks of both V_{Zn}-ZIS and UCNPs, which are consistent with the element mapping results of SEM images. The ultraviolet-visible (UV-vis) diffuse reflectance spectra (DRS) were adopted to evaluate the light absorption capability of different samples. As shown in Figure 3B, V_{Zn}-ZIS possesses a broad ultraviolet to visible light absorption (from 200 to 700 nm). Although pristine UCNPs have weak absorbance in the visible light region, they exhibit two obvious absorption peaks around 753 and 967 nm. The composite of UCNPs@V_{Zn}-ZIS well maintains the advantages of both UCNPs and V_{Zn}-ZIS after combining V_{Zn}-ZIS with UCNPs. Specifically, UCNPs@V_{Zn}-ZIS not only can absorb light from 200 to 570 nm but also exhibits absorption peaks at the NIR region around 727 and 976 nm, respectively. X-ray photoelectron spectroscopy (XPS) spectra are shown in Figure 3C-E. Compared with pure V_{Zn}-ZIS, the Zn 2p and In 3d of UCNPs@V_{Zn}-ZIS moved to higher binding energy while S 2p moved to lower. In addition, as shown in Supplementary Figure 5A-E, Na 1s, Y 3d, F 1s, Yb 4d and Er 4d of UCNPs moved to higher binding energy region after mixing with V_{Zn}-ZIS, proving the strong interaction between V_{Zn}-ZIS and UCNPs[34]. Additionally, the concentration of Zn vacancies of V_{Zn}-ZIS was calculated according to the XPS spectra of Zn 2p and In 3d [Supplementary Table 1] . As shown in Figure 3F, the g value of 2.004 proves the existence of Zn vacancies in V_{Zn}-ZIS[35]. In addition, the higher intensity demonstrates that V_{Zn}-ZIS possesses a higher Zn vacancy concentration than ZIS. Compared with ZIS, Zn 2p and S 2p of V_{Zn}-ZIS shift to a lower binding energy region [Supplementary Figure 6A and B], which also demonstrates the existence of Zn vacancies[26].

Photocatalytic performance

The photocatalytic CO_2 reduction process was conducted under NIR irradiation (800-1,100 nm) using triethanolamine as the sacrificial agent. As a result, the CO evolution of UCNPs@V_{Zn}-ZIS was up to 32.57 μmol/g under NIR light irradiation for 8 h, which was six times of pristine V_{Zn}-ZIS and about 16 times of UCNPs@ZIS [Figure 4A]. The enhanced photocatalytic CO_2 reduction performance of UCNPs@V_{Zn}-ZIS was attributed to the enhanced light absorption region, increased Zn vacancy, and the up-conversion light

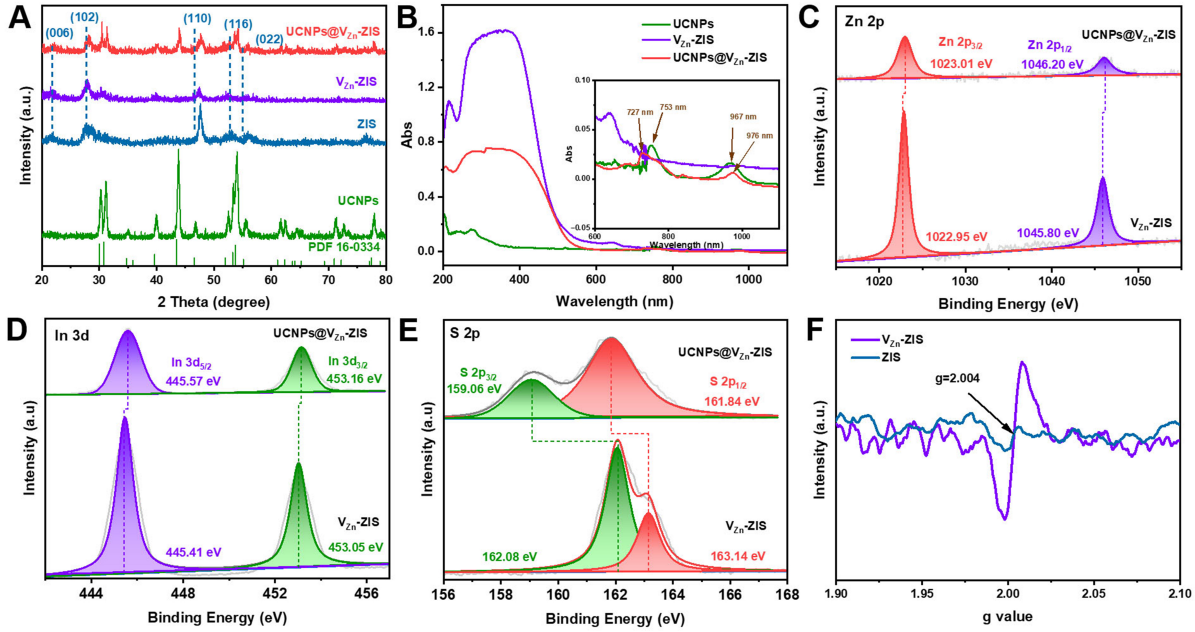

Figure 3. (A) XRD patterns of ZIS, V_{Zn}-ZIS, UCNPs, and UCNPs@V_{Zn}-ZIS; (B) DRS of V_{Zn}-ZIS, UCNPs, and UCNPs@V_{Zn}-ZIS; XPS spectra of Zn 2p, In 3d and S 2p of V_{Zn}-ZIS and UCNPs@V_{Zn}-ZIS (C-E); (F) EPR signals of ZIS and V_{Zn}-ZIS. XRD: X-ray diffraction; ZIS: $ZnIn_2S_4$; V_{Zn}-ZIS: Zn vacancy-rich $ZnIn_2S_4$; UCNPs: up-conversion nanoparticles; DRS: diffuse reflectance spectra; XPS: X-ray photoelectron spectroscopy; EPR: electron paramagnetic resonance.

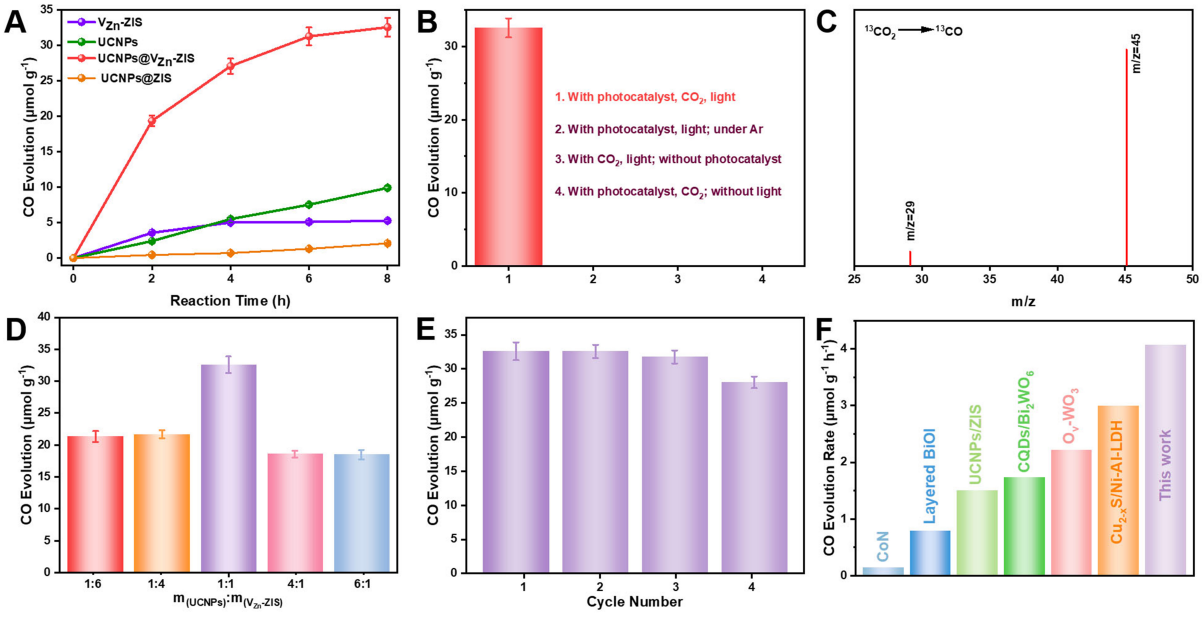

Figure 4. (A) CO evolution over time of V_{Zn}-ZIS, UCNPs, UCNPs@V_{Zn}-ZIS and UCNPs@ZIS; (B) Controlled photocatalytic CO_2 reduction experiments in the absence of CO_2, light or photocatalyst; (C) Carbon labeling experiment of the generated product using $^{13}CO_2$ as the feed gas; (D) Photocatalytic CO_2 reduction activity of UCNPs@V_{Zn}-ZIS with different mass ratio; (E) Photocatalytic stability test of UCNPs@V_{Zn}-ZIS; (F) Comparison of CO generation rate under NIR irradiation of UCNPs@V_{Zn}-ZIS with recent reported photocatalysts. V_{Zn}-ZIS: Zn vacancy-rich $ZnIn_2S_4$; UCNPs: up-conversion nanoparticles; NIR: near-infrared.

emission induced by UCNPs. In detail, UCNPs can absorb NIR light and emit visible light to activate V_{Zn}-ZIS for CO_2 reduction. Moreover, a series of controlled experiments were conducted in Figure 4B to investigate the source of products of photocatalytic CO_2 reduction. As a result, no CO was generated in the absence of a photocatalyst, light, or CO_2 in the photocatalytic system. To further clarify the source of CO, a carbon labeling experiment was conducted by using $^{13}CO_2$ as feed gas. As shown in Figure 4C, a signal of m/z = 29 can be observed, implying that ^{13}CO was generated from $^{13}CO_2$ (m/z = 45). In addition, the mass ratio of UCNPs and V_{Zn}-ZIS in the composite of UCNPs@V_{Zn}-ZIS was adjusted to optimize the efficiency of photocatalytic CO_2 reduction [Figure 4D]. As a result, when the mass ratio of UCNPs is equal to V_{Zn}-ZIS, the UCNPs@V_{Zn}-ZIS exhibited much higher CO evolution than other controls. The trade-off effect of UCNPs loading on V_{Zn}-ZIS may cause insufficient exposure to photocatalytic active sites. Moreover, a recycling test was conducted to evaluate the photocatalytic stability of UCNPs@V_{Zn}-ZIS. As shown in Figure 4E, the CO generation shows no obvious change after four photocatalytic cycles, demonstrating the superior stability of UCNPs@V_{Zn}-ZIS. Besides, the SEM image [Supplementary Figure 9] and XRD spectra [Supplementary Figure 10] of UCNPs@V_{Zn}-ZIS after the recycling test remain unchanged when compared with fresh photocatalysts, further proving the photostability of UCNPs@V_{Zn}-ZIS. Furthermore, CO generation rates of different photocatalysts in the literature under NIR irradiation were also compared in Figure 4F. Specifically, the UCNPs@V_{Zn}-ZIS in this work exhibits a much higher generation rate than other reports[18,36-40].

Photocatalytic charge separation

A series of characterizations were utilized to evaluate the charge separation and migration behaviors of photocatalysts, including photoluminescence (PL), PL decay curves, laser scanning confocal microscopy (LSCM) images, surface photovoltage (SPV), transient photocurrent and EIS. As shown in Figure 5A, pure UCNPs exhibit several up-conversion PL emission peaks of 410, 525, 546, and 660 nm when excited by a laser of 980 nm. The detailed luminescence emission process of UCNPs was described in the part of the mechanism of photocatalytic CO_2 reduction. As shown in Figure 5B, UCNPs@V_{Zn}-ZIS displays lower PL intensity than pristine V_{Zn}-ZIS and UCNPs, indicating the decreased charge recombination efficiency[41]. The average PL decay lifetime of V_{Zn}-ZIS, UCNPs, and UCNPs@V_{Zn}-ZIS is 3.85, 5.84, and 5.87 ns, respectively [Figure 5C]. The increased PL decay time of UCNPs@V_{Zn}-ZIS reveals a longer lifetime of charge carriers and better separation of photo-induced electrons and holes[42]. The LSCM result of V_{Zn}-ZIS [Figure 5D and E] shows a much brighter image than UCNPs@V_{Zn}-ZIS, indicating a lower recombination rate of photo-induced charges in UCNPs@V_{Zn}-ZIS. In addition, more photo-generated electrons of UCNPs@V_{Zn}-ZIS can be transferred for further photocatalytic CO_2 reductions. The SPV spectra [Figure 5F] of UCNPs@V_{Zn}-ZIS exhibit higher SPV response than V_{Zn}-ZIS and UCNPs, implying that more photo-generated electrons can be generated and migrated to the surface of UCNPs@V_{Zn}-ZIS[43]. The transient photocurrent response of UCNPs@V_{Zn}-ZIS [Figure 5G] is higher than V_{Zn}-ZIS and UCNPs, which is consistent with the SPV results. Moreover, UCNPs@V_{Zn}-ZIS demonstrates a smaller EIS semicircle than V_{Zn}-ZIS and UCNPs [Figure 5H], indicating a lower migration resistance.

Mechanism of photocatalytic CO_2 reduction

The specific band positions of the photocatalysts were investigated by the MS and the Tauc plot. According to MS curves in Figure 6A, the slope of V_{Zn}-ZIS is positive, belonging to the n-type semiconductor[44]. Specifically, the flat potential of V_{Zn}-ZIS is -0.90 V (*vs.* Ag/AgCl). Therefore, the potential of the conduction band (CB) of V_{Zn}-ZIS is -0.90 eV [*vs.* normal hydrogen electrode (NHE)][26]. As shown in the Tauc plot in Figure 6B, the energy of the band gap (E_g) of V_{Zn}-ZIS is 2.69 eV. According to $E_g = |E_{CB}-E_{VB}|$, the potential of the valence band of V_{Zn}-ZIS is calculated as 1.79 eV (*vs.* NHE).

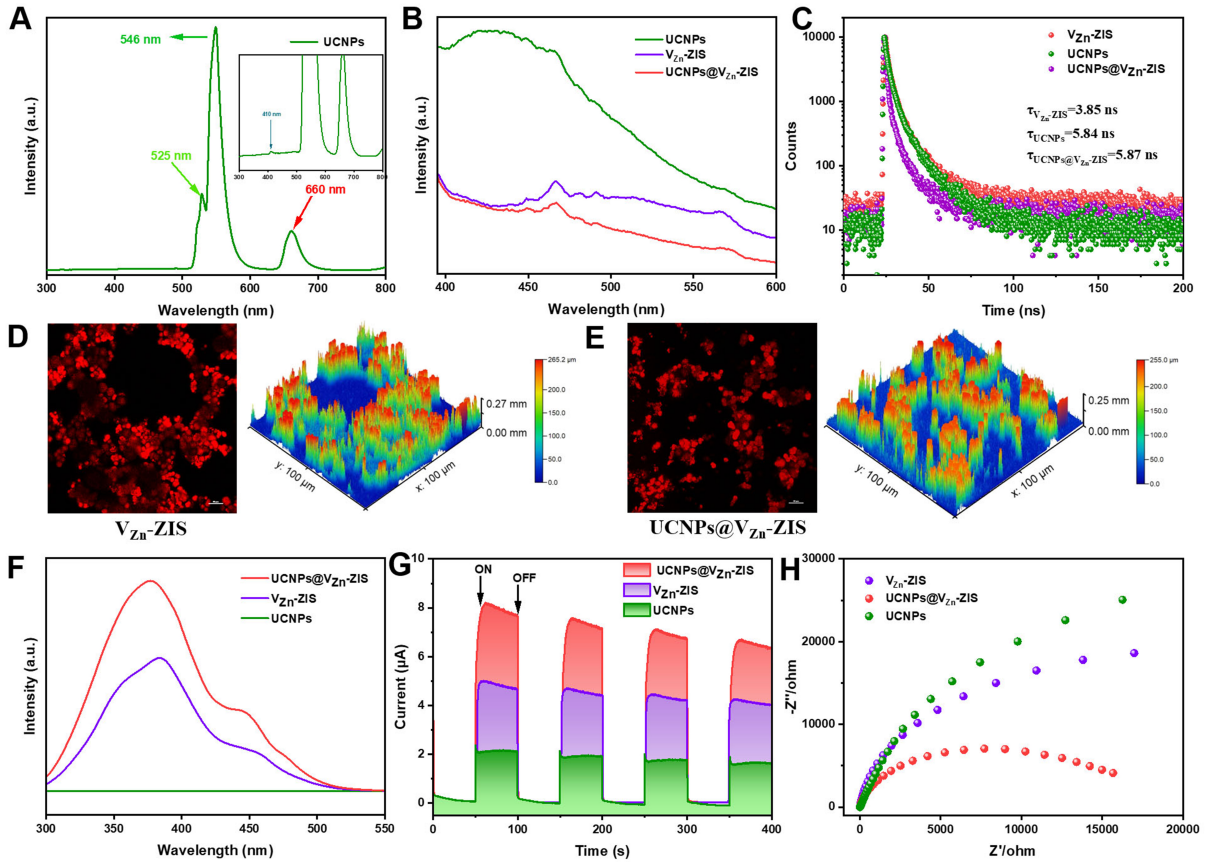

Figure 5. (A) PL curve of pure UCNPs when excited by a laser of 980 nm; (B) PL emission spectra of V_{Zn}-ZIS, UCNPs, and UCNPs@V_{Zn}-ZIS under the excitation of 350 nm; (C) PL decay curves of V_{Zn}-ZIS, UCNPs and UCNPs@V_{Zn}-ZIS; LSCM images of V_{Zn}-ZIS (D) and UCNPs@V_{Zn}-ZIS (E); (F) SPV spectra of V_{Zn}-ZIS, UCNPs and UCNPs@V_{Zn}-ZIS; Transient photocurrent (G) and EIS Nyquist plots (H) of V_{Zn}-ZIS, UCNPs and UCNPs@V_{Zn}-ZIS. PL: Photoluminescence; UCNPs: up-conversion nanoparticles; V_{Zn}-ZIS: Zn vacancy-rich $ZnIn_2S_4$; LSCM: laser scanning confocal microscopy; SPV: surface photovoltage; EIS: electrochemical impedance spectroscopy.

To clarify the mechanism of photocatalytic CO_2 reduction of UCNPs@V_{Zn}-ZIS, *in-situ* Fourier transform infrared (*in-situ* FTIR) spectroscopy was adopted to test the reaction intermediates. As shown in Figure 6C, no peak exists in the absence of light and CO_2. After introducing CO_2 under irradiation, new peaks occurred and strengthened with the prolonged reaction time. In detail, the peak at 1,727 cm^{-1} belonged to the C=O bond, indicating that CO_2 was successfully introduced to the system[45]. Besides, monodentate carbonate species (m-CO_3^{2-}, 1,547, 1,488, 1,475, and 1,375 cm^{-1}) and bidentate carbonate species (b-CO_3^{2-}, 1,658, and 1,315 cm^{-1}) were detected and increased with the increased irradiation time, proving that CO_2 was dissolved in water (H_2O, 1,641 cm^{-1})[46-49]. Moreover, the peaks of other carbon-based species such as bicarbonate species (HCO_3^-, 1,453, 1,416, and 1,398 cm^{-1}), carboxylate species (COO^-, 1,565, 1,363, and 1,338 cm^{-1}), carboxyl ($^*COOH$, 1,679, 1,527, and 1,288 cm^{-1}) and formaldehyde species ($HCHO^-$, 1,781 and 1,511 cm^{-1}) also appeared during the process of photocatalytic CO_2 reduction, proving these intermediates were produced on the surface of UCNPs@V_{Zn}-ZIS[46,50-52]. Notably, $^*COOH$ is a significant intermediate of reducing CO_2 to CO according to the previous study[51]. These intermediates prove that the photocatalytic process of CO_2 reduction occurred on the surface of UCNPs@V_{Zn}-ZIS.

The mechanism of up-conversion-induced photocatalytic CO_2 reduction of UCNPs@V_{Zn}-ZIS is shown in Figure 6D. The $UCNP_S$ can emit green luminescence (546 and 525 nm) and red luminescence (660 nm)

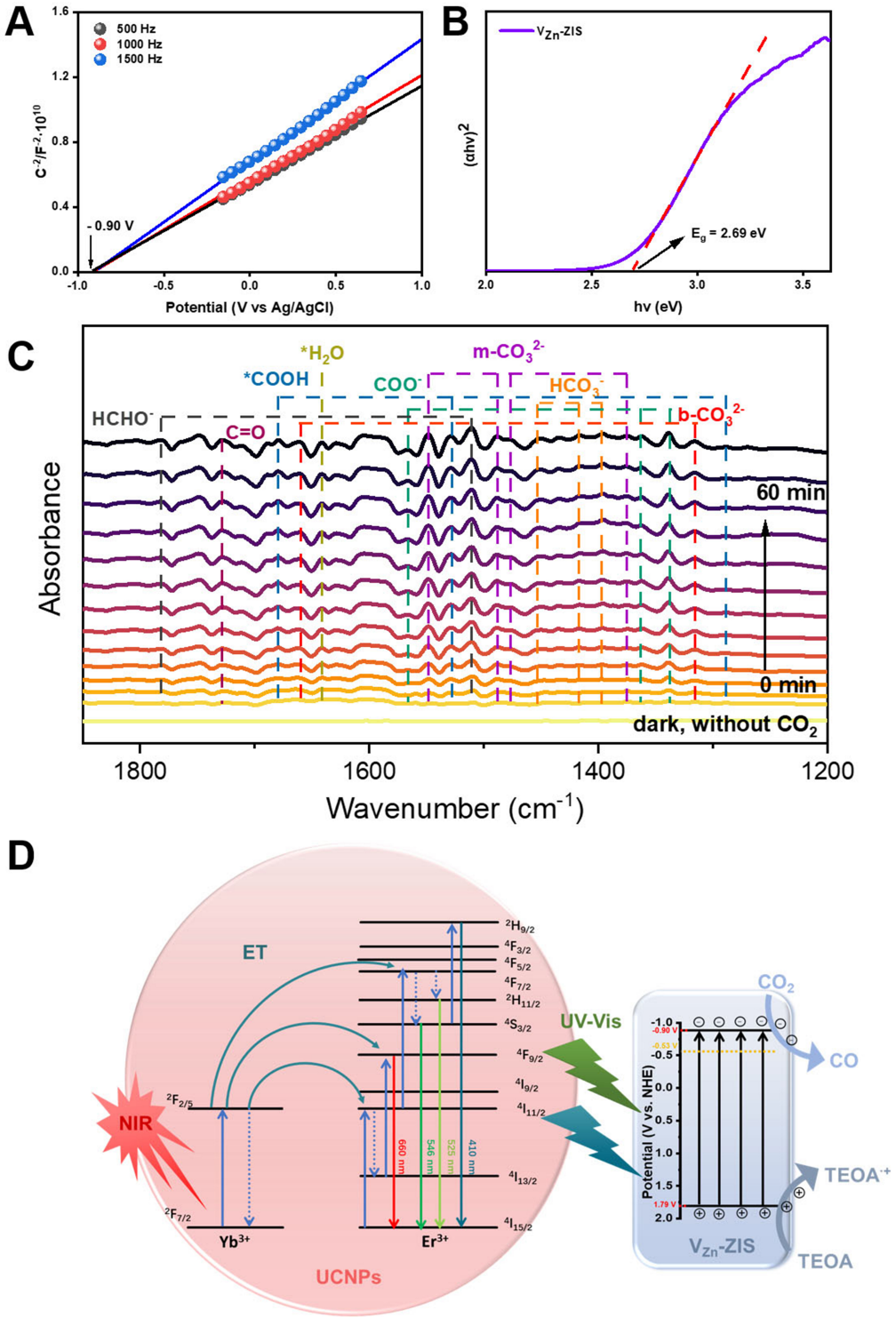

Figure 6. (A) MS curves and (B) Tauc plot of V_{Zn}-ZIS; (C) *In-situ* FTIR spectra of UCNPs@V_{Zn}-ZIS; (D) Photocatalytic CO_2 reduction mechanism on UCNPs@V_{Zn}-ZIS under the NIR light irradiation. MS: Mott-Schottky; V_{Zn}-ZIS: Zn vacancy-rich $ZnIn_2S_4$; *in-situ* FTIR: *in-situ* Fourier transform infrared; UCNPs: up-conversion nanoparticles; NIR: near-infrared.

under the excitation of an infrared laser of 980 nm [Figure 5A]. In detail, the up-conversion generated red luminescence at 660 nm comprised three steps of energy transfer (ET) from Yb^{3+} to Er^{3+}[53]. Firstly, Yb^{3+} ions

are excited from the ground state ($^2F_{7/2}$) to the excited state ($^2F_{5/2}$) after absorbing photons from a laser of 980 nm[54]. Subsequently, Er^{3+} ions were excited from the ground state ($^4I_{15/2}$) to the excited state ($^4F_{11/2}$) through the ET from adjacent Yb^{3+}. Secondly, $^4F_{13/2}$ of Er^{3+} was filled through a nonradiative relaxation from $^4F_{11/2}$ to $^4I_{13/2}$. Thirdly, another ET of adjacent Yb^{3+} took place, which caused Er^{3+} in the $^4I_{13/2}$ state to be excited to the $^4F_{9/2}$ state[52]. To return to the ground state, Er^{3+} ions in the $^4F_{9/2}$ state release the energy and emit red luminescence at 660 nm simultaneously[55]. As for the green luminescence, the $^4F_{7/2}$ state of Er^{3+} was filled first with two ET of adjacent Yb^{3+} ions. Subsequently, Er^{3+} can emit green luminescence at 525 and 546 nm through a nonradiative relaxation from $^4F_{7/2}$ to $^2H_{11/2}$ and $^4S_{3/2}$, accordingly[55]. However, the $^2H_{9/2}$ of Er^{3+} can hardly be filled through ET of Yb^{3+} because of the energy mismatch, so the intensity of luminescence of 410 nm was weak. The green luminescence (525 and 546 nm) emitted from $UCNP_S$ can be absorbed by V_{Zn}-ZIS according to DRS in Figure 3B. Then, V_{Zn}-ZIS was excited to generate e^--h^+ pairs. Due to the energy of CB (E_{CB}) of V_{Zn}-ZIS (-0.90 V) being more negative than the potential of reducing CO_2 to CO (-0.53 V), the photocatalytic CO_2 reduction reaction on V_{Zn}-ZIS is thermodynamically feasible.

CONCLUSIONS

In summary, a nanoflower-shaped UCNPs@V_{Zn}-ZIS photocatalyst was successfully synthesized through a facile physical mixing approach. With the green light emitted from up-conversion, V_{Zn}-ZIS was activated and e^--h^+ pairs for photocatalytic CO_2 reduction were generated. The obtained UCNPs@V_{Zn}-ZIS demonstrates a superior CO evolution under pure NIR light irradiation. The enhanced CO evolution of UCNPs@V_{Zn}-ZIS was attributed to strengthened light harvesting, improved CO_2 activation of the surface vacancy, and enhanced e^--h^+ pairs separation efficiency. The work presented here provides a facile approach to developing novel broad spectral responsive photocatalytic CO_2 reduction photocatalysts, which hold great potential for solar fuel generation in future applications.

DECLARATIONS

Authors' contributions

Validation, formal analysis, investigation, resources, data curation, writing - original draft: Li, X.; Wu, H.
Data curation: Yin, S.
Validation, formal analysis: Yu, C.
Data curation: Shao, Y.
Writing - review and editing: Zhou, D.
Conceptualization, validation, writing - review and editing: She, P.

Availability of data and materials

Experimental procedures and characterizations of photocatalysts are available in the Supplementary Materials. Further data is available from the corresponding authors upon reasonable request.

Financial support and sponsorship

This study was funded by the Department of Education of Jilin Province (JJKH20241250KJ), the National Natural Science Foundation of China (Grant Nos. 22301099 and 22279041), the National Key Research and Development Program of China (No. 2022YFC2105800) and the 111 Project (B17020).

Conflicts of interest

All authors declared that there are no conflicts of interest.

Ethical approval and consent to participate

Not applicable.

Consent for publication

Not applicable.

REFERENCES

1. Achakulwisut, P.; Erickson, P.; Guivarch, C.; Schaeffer, R.; Brutschin, E.; Pye, S. Global fossil fuel reduction pathways under different climate mitigation strategies and ambitions. *Nat. Commun.* **2023**, *14*, 5425. DOI PubMed PMC
2. air for a sustainable world. *Nat. Commun.* **2021**, *12*, 5824. DOI PubMed PMC
3. Fang, S.; Rahaman, M.; Bharti, J.; et al. Photocatalytic CO_2 reduction. *Nat. Rev. Methods. Primers.* **2023**, *3*, 243. DOI
4. Albero, J.; Peng, Y.; García, H. Photocatalytic CO_2 reduction to C2+ products. *ACS. Catal.* **2020**, *10*, 5734-49. DOI
5. Bhanderi, D.; Lakhani, P.; Modi, C. K. Graphitic carbon nitride (g-C_3N_4) as an emerging photocatalyst for sustainable environmental applications: a comprehensive review. *RSC. Sustain.* **2024**, *2*, 265-87. DOI
6. Yang, R.; Mei, L.; Fan, Y.; et al. $ZnIn_2S_4$-based photocatalysts for energy and environmental applications. *Small. Methods.* **2021**, *5*, e2100887. DOI
7. Li, Z.; Li, Z.; Zuo, C.; Fang, X. Application of nanostructured TiO_2 in UV photodetectors: a review. *Adv. Mater.* **2022**, *34*, e2109083. DOI
8. Yang, M. Q.; Gao, M.; Hong, M.; Ho, G. W. Visible-to-NIR photon harvesting: progressive engineering of catalysts for solar-powered environmental purification and fuel production. *Adv. Mater.* **2018**, *30*, e1802894. DOI PubMed
9. Han, C.; Kundu, B. K.; Liang, Y.; Sun, Y. Near-infrared light-driven photocatalysis with an emphasis on two-photon excitation: concepts, materials, and applications. *Adv. Mater.* **2024**, *36*, e2307759. DOI
10. Xu, M.; Ruan, X.; Meng, D.; et al. Modulation of sulfur vacancies in $ZnIn_2S_4$/MXene Schottky heterojunction photocatalyst promotes hydrogen evolution. *Adv. Funct. Mater.* **2024**, *34*, 2402330. DOI
11. Peng, H.; Yang, H.; Han, J.; et al. Defective $ZnIn_2S_4$ nanosheets for visible-light and sacrificial-agent-free H_2O_2 photosynthesis via O_2/H_2O redox. *J. Am. Chem. Soc.* **2023**, *145*, 27757-66. DOI
12. Sun, L.; Wang, W.; Kong, T.; Jiang, H.; Tang, H.; Liu, Q. Fast charge transfer kinetics in an inorganic–organic S-scheme heterojunction photocatalyst for cooperative hydrogen evolution and furfuryl alcohol upgrading. *J. Mater. Chem. A.* **2022**, *10*, 22531-9. DOI
13. Qiu, B.; Huang, P.; Lian, C.; et al. Realization of all-in-one hydrogen-evolving photocatalysts via selective atomic substitution. *Appl. Catal. B. Environ.* **2021**, *298*, 120518. DOI
14. Tian, Q.; Yao, W.; Wu, W.; et al. Efficient UV–Vis-NIR responsive upconversion and plasmonic-enhanced photocatalyst based on lanthanide-doped $NaYF_4$/SnO_2/Ag. *ACS. Sustainable. Chem. Eng.* **2017**, *5*, 10889-99. DOI
15. Huang, H.; Liang, X.; Wang, Z.; et al. $Bi_{20}TiO_{32}$ nanoparticles doped with Yb^{3+} and Er^{3+} as UV, visible, and near-infrared responsive photocatalysts. *ACS. Appl. Nano. Mater.* **2019**, *2*, 5381-8. DOI
16. Xie, J.; Zhang, X.; Lu, Z.; et al. Up-conversion effect boosted the photocatalytic CO_2 reduction activity of Z-scheme CPDs/BiOBr heterojunction. *Inorg. Chem. Front.* **2023**, *10*, 5127-35. DOI
17. Wen, S.; Zhou, J.; Zheng, K.; Bednarkiewicz, A.; Liu, X.; Jin, D. Advances in highly doped upconversion nanoparticles. *Nat. Commun.* **2018**, *9*, 2415. DOI PubMed PMC
18. Yu, M.; Lv, X.; Mahmoud, I. A.; et al. Upconversion nanoparticles coupled with hierarchical $ZnIn_2S_4$ nanorods as a near-infrared responsive photocatalyst for photocatalytic CO_2 reduction. *J. Colloid. Interface. Sci.* **2022**, *612*, 782-91. DOI
19. Hou, Z.; Zhang, Y.; Deng, K.; et al. UV-emitting upconversion-based TiO_2 photosensitizing nanoplatform: near-infrared light mediated in vivo photodynamic therapy via mitochondria-involved apoptosis pathway. *ACS. Nano.* **2015**, *9*, 2584-99. DOI
20. Nie, Z.; Ke, X.; Li, D.; et al. $NaYF_4$:Yb,Er,Nd@$NaYF_4$:Nd upconversion nanocrystals capped with Mn:TiO_2 for 808 nm NIR-triggered photocatalytic applications. *J. Phys. Chem. C.* **2019**, *123*, 22959-70. DOI
21. Karami, A.; Farivar, F.; de, P. T. J.; et al. Facile multistep synthesis of ZnO-coated β-$NaYF_4$:Yb/Tm upconversion nanoparticles as an antimicrobial photodynamic therapy for persistent *Staphylococcus aureus* small colony variants. *ACS. Appl. Bio. Mater.* **2021**, *4*, 6125-36. DOI
22. Liu, Q.; Wu, B.; Li, M.; Huang, Y.; Li, L. Heterostructures made of upconversion nanoparticles and metal-organic frameworks for biomedical applications. *Adv. Sci.* **2022**, *9*, e2103911. DOI PubMed PMC
23. Cheng, Q.; Huang, M.; Xiao, L.; et al. Unraveling the influence of oxygen vacancy concentration on electrocatalytic CO_2 reduction to formate over indium oxide catalysts. *ACS. Catal.* **2023**, *13*, 4021-9. DOI
24. Peng, C.; Luo, G.; Zhang, J.; et al. Double sulfur vacancies by lithium tuning enhance CO_2 electroreduction to n-propanol. *Nat. Commun.* **2021**, *12*, 1580. DOI PubMed PMC
25. Zhang, K.; Dan, M.; Yang, J.; et al. Surface energy mediated sulfur vacancy of $ZnIn_2S_4$ atomic layers for photocatalytic H_2O_2 production. *Adv. Funct. Mater.* **2023**, *33*, 2302964. DOI
26. He, Y.; Rao, H.; Song, K.; et al. 3D hierarchical $ZnIn_2S_4$ nanosheets with rich Zn vacancies boosting photocatalytic CO_2 reduction.

Adv. Funct. Mater. **2019**, *29*, 1905153. DOI

27. Nie, Y.; Bo, T.; Zhou, W.; et al. Understanding the role of Zn vacancy induced by sulfhydryl coordination for photocatalytic CO_2 reduction on $ZnIn_2S_4$. *J. Mater. Chem. A.* **2023**, *11*, 1793-800. DOI
28. Zhang, G.; Wu, H.; Chen, D.; et al. A mini-review on $ZnIn_2S_4$-based photocatalysts for energy and environmental application. *Green. Energy. Environ.* **2022**, *7*, 176-204. DOI
29. Ouyang, C.; Quan, X.; Chen, Z. A.; et al. Intercalation- and vacancy-enhanced internal electric fields in $ZnIn_2S_4$ for highly efficient photocatalytic H_2O_2 production. *J. Phys. Chem. C.* **2023**, *127*, 20683-99. DOI
30. Zhang, Z.; Liu, K.; Feng, Z.; Bao, Y.; Dong, B. Hierarchical sheet-on-sheet $ZnIn_2S_4$/g-C_3N_4 heterostructure with highly efficient photocatalytic H_2 production based on photoinduced interfacial charge transfer. *Sci. Rep.* **2016**, *6*, 19221. DOI PubMed PMC
31. Xin, Z.; Zheng, H.; Hu, J. Construction of hollow Co_3O_4@$ZnIn_2S_4$ p-n heterojunctions for highly efficient photocatalytic hydrogen production. *Nanomaterials* **2023**, *13*, 758. DOI PubMed PMC
32. Qiu, H.; Tan, M.; Ohulchanskyy, T. Y.; Lovell, J. F.; Chen, G. Recent progress in upconversion photodynamic therapy. *Nanomaterials* **2018**, *8*, 344. DOI PubMed PMC
33. Si, S.; Shou, H.; Mao, Y.; et al. Low-coordination single Au atoms on ultrathin $ZnIn_2S_4$ nanosheets for selective photocatalytic CO_2 reduction towards CH_4. *Angew. Chem. Int. Ed. Engl.* **2022**, *61*, e202209446. DOI
34. Chong, W. K.; Ng, B. J.; Lee, Y. J.; et al. Self-activated superhydrophilic green $ZnIn_2S_4$ realizing solar-driven overall water splitting: close-to-unity stability for a full daytime. *Nat. Commun.* **2023**, *14*, 7676. DOI PubMed PMC
35. Xu, B.; Li, H.; Chong, B.; Lin, B.; Yan, X.; Yang, G. Zn vacancy-tailoring mediated $ZnIn_2S_4$ nanosheets with accelerated orderly charge flow for boosting photocatalytic hydrogen evolution. *Chem. Eng. Sci.* **2023**, *270*, 118533. DOI
36. Liang, L.; Li, X.; Zhang, J.; et al. Efficient infrared light induced CO_2 reduction with nearly 100% CO selectivity enabled by metallic CoN porous atomic layers. *Nano. Energy.* **2020**, *69*, 104421. DOI
37. Ye, L.; Wang, H.; Jin, X.; et al. Synthesis of olive-green few-layered BiOI for efficient photoreduction of CO_2 into solar fuels under visible/near-infrared light. *Sol. Energ. Mat. Sol. C.* **2016**, *144*, 732-9. DOI
38. Kong, X. Y.; Tan, W. L.; Ng, B.; Chai, S.; Mohamed, A. R. Harnessing Vis–NIR broad spectrum for photocatalytic CO_2 reduction over carbon quantum dots-decorated ultrathin Bi_2WO_6 nanosheets. *Nano. Res.* **2017**, *10*, 1720-31. DOI
39. Liang, L.; Li, X.; Sun, Y.; et al. Infrared light-driven CO_2 overall splitting at room temperature. *Joule* **2018**, *2*, 1004-16. DOI
40. Ji, X.; Guo, R.; Tang, J.; et al. Construction of full solar-spectrum-driven $Cu_{2-x}S$/Ni-Al-LDH heterostructures for efficient photocatalytic CO_2 reduction. *ACS. Appl. Energy. Mater.* **2022**, *5*, 2862-72. DOI
41. Wang, F.; Chen, S.; Wu, J.; Xiang, W.; Duan, L. Construction of 2D/3D g-C_3N_4/$ZnIn_2S_4$ heterojunction for efficient photocatalytic reduction of CO_2 under visible light. *Ind. Eng. Chem. Res.* **2023**, *62*, 15907-18. DOI
42. Ji, J.; Li, R.; Zhang, H.; et al. Highly selective photocatalytic reduction of CO_2 to ethane over Au-O-Ce sites at micro-interface. *Appl. Catal. B. Environ.* **2023**, *321*, 122020. DOI
43. Hu, T.; Feng, P.; Guo, L.; Chu, H.; Liu, F. Construction of built-in electric field in TiO_2@Ti_2O_3 core-shell heterojunctions toward optimized photocatalytic performance. *Nanomaterials* **2023**, *13*, 2125. DOI PubMed PMC
44. Ouyang, C.; Quan, X.; Zhang, C.; et al. Direct Z-scheme $ZnIn_2S_4$@MoO_3 heterojunction for efficient photodegradation of tetracycline hydrochloride under visible light irradiation. *Chem. Eng. J.* **2021**, *424*, 130510. DOI
45. Böke, J. S.; Popp, J.; Krafft, C. Optical photothermal infrared spectroscopy with simultaneously acquired Raman spectroscopy for two-dimensional microplastic identification. *Sci. Rep.* **2022**, *12*, 18785. DOI PubMed PMC
46. Wang, L.; Cheng, B.; Zhang, L.; Yu, J. In situ irradiated XPS investigation on S-scheme TiO_2@$ZnIn_2S_4$ photocatalyst for efficient photocatalytic CO_2 reduction. *Small* **2021**, *17*, e2103447. DOI
47. Shangguan, W.; Liu, Q.; Wang, Y.; et al. Molecular-level insight into photocatalytic CO_2 reduction with H_2O over Au nanoparticles by interband transitions. *Nat. Commun.* **2022**, *13*, 3894. DOI PubMed PMC
48. Wang, B.; Zhang, W.; Liu, G.; et al. Excited electron-rich $Bi^{(3-x)+}$ sites: a quantum well-like structure for highly promoted selective photocatalytic CO_2 reduction performance. *Adv. Funct. Mater.* **2022**, *32*, 2202885. DOI
49. Pogorelov, V.; Doroshenko, I.; Pitsevich, G.; et al. From clusters to condensed phase - FT IR studies of water. *J. Mol. Liq.* **2017**, *235*, 7-10. DOI
50. Ran, L.; Li, Z.; Ran, B.; et al. Engineering single-atom active sites on covalent organic frameworks for boosting CO_2 photoreduction. *J. Am. Chem. Soc.* **2022**, *144*, 17097-109. DOI
51. Ma, Y.; Zhang, Y.; Xie, G.; et al. Isolated Cu sites in CdS hollow nanocubes with doping-location-dependent performance for photocatalytic CO_2 reduction. *ACS. Catal.* **2024**, *14*, 1468-79. DOI
52. Zhang, J.; Cao, C.; Wang, J.; Li, S.; Xie, Y. $NaYF_4$:Yb,Er@$NaYF_4$:Yb,Tm and $NaYF_4$:Yb,Tm@$NaYF_4$:Yb,Er core@shell upconversion nanoparticles embedded in acrylamide hydrogels for anti-counterfeiting and information encryption. *ACS. Appl. Nano. Mater.* **2022**, *5*, 16642-54. DOI
53. Chen, G.; Qiu, H.; Prasad, P. N.; Chen, X. Upconversion nanoparticles: design, nanochemistry, and applications in theranostics. *Chem. Rev.* **2014**, *114*, 5161-214. DOI PubMed PMC
54. Ansari, A. A.; Labis, J. P.; Khan, A. Biocompatible $NaYF_4$:Yb,Er upconversion nanoparticles: colloidal stability and optical properties. *J. Saudi. Chem. Soc.* **2021**, *25*, 101390. DOI
55. Giang, L. T. K.; Trejgis, K.; Marciniak, L.; Vu, N.; Minh, L. Q. Fabrication and characterization of up-converting β-$NaYF_4$:Er^{3+},Yb^{3+}@$NaYF_4$ core-shell nanoparticles for temperature sensing applications. *Sci. Rep.* **2020**, *10*, 14672. DOI PubMed PMC

Xuejing Li

Xuejing Li is a postgraduate student at the State Key Laboratory of Inorganic Synthesis and Preparative Chemistry of Jilin University. She received her B.S. degree in Chemistry from Shandong Normal University in 2023. Her current research focuses on inorganic semiconductors and their applications in photocatalytic carbon dioxide reduction and hydrogen evolution.

Haiyue Wu

Haiyue Wu received her B.S. degree in the School of Chemistry at Jilin University in 2024. Her current research focuses on inorganic semiconductors and their applications in photocatalysis carbon dioxide reduction.

Shengyan Yin

Shengyan Yin graduated from the State Key Laboratory of Supramolecular Structures and Materials of Jilin University and obtained his Doctor of Science degree in 2009. From 2009 to 2013, he conducted postdoctoral research in Nanyang Technological University, Singapore (co-supervisor: Academician Chen Xiaodong). In August 2013, he joined the School of Electronic Science and Engineering of Jilin University as an academic backbone and was hired as a professor in 2018. He is mainly engaged in the application research of graphene materials in biomedicine (including the integration research of tumor diagnosis and treatment, the isolation and detection of circulating tumor cells, biosensing and drug delivery research).

Chenhao Yu

Chenhao Yu is a student at the State Key Laboratory of Integrated Optoelectronics at Jilin University. He graduated with a master's degree from the National Laboratory of Supramolecular Structures and Materials. His current research focuses on the hydrogen-producing properties of organic polymer materials.

Yongzhi Shao

Yongzhi Shao is a graduate student at the School of Electronic Science and Engineering, Jilin University. He received his Master's degree in Integrated Circuit Engineering from Jilin University in 2024. His research focuses on the synthesis and preparation of rare-earth-doped perovskite quantum dots.

Donglei Zhou

Donglei Zhou graduated from the College of Electronic Science and Engineering of Jilin University in 2013. He received his Ph.D. in 2018. Now, He is a professor in the College of Electronic Science and Engineering of Jilin University. He is mainly engaged in the research of rare earth luminescent materials, optoelectronic materials and devices.

Ping She

Ping She is currently an assistant professor at the College of Chemistry of Jilin University. She received a bachelor's degree from Jilin University in 2014. In 2018, she obtained her Ph.D. in engineering from Jilin University. She then completed postdoctoral work at Jilin University (Post Doctoral Innovative Talent Support Program of China from 2018 to 2021). Her research focuses on inorganic porous nanomaterial-based catalysis evolution.